PHYSICAL REVIEW B

CONDENSED MATTER

THIRD SERIES, VOLUME 37, NUMBER 10 PART A 1 APRIL 1988

ESR pumping experiments in spin-polarized atomic hydrogen

A. P. M. Mattheij,* J. van Zwol,† and J. T. M. Walraven
Natuurkundig Laboratorium, Universiteit van Amsterdam, Valckenierstraat 65, NL-1018 XE Amsterdam, The Netherlands

Isaac F. Silvera
Lyman Laboratory of Physics, Harvard University, Cambridge, Massachusetts 02138
(Received 29 June 1987)

Pumping experiments were carried out in atomic hydrogen using an ESR technique. A model of the decay of the four hyperfine states in the presence of a moderately strong resonant microwave field is described and compared with experimental results. The results indicate that because of spin-exchange relaxation, it is difficult to influence the nuclear polarization of the lower hyperfine states by means of ESR pumping. The model is applied to the design of an ESR-operated beam source of spin-polarized atomic hydrogen. We estimate that in our experiments the maximum flux of particles ejected from the source was 5×10^{13} sec^{-1}.

I. INTRODUCTION

Electron spin resonance (ESR) has proven to be a valuable tool in the study of the decay kinetics of spin-polarized atomic hydrogen. Using ESR, the densities in the lower hyperfine states may be determined separately. ESR has been successfully applied in the study of various magnetic relaxation and recombination processes,[1-4] and to observe atomic hydrogen in a surface bound state.[3] Alternatively, instead of using ESR as a detection scheme, it may be applied at a high-power level to directly influence the populations of the hyperfine states. In a strong resonant microwave field, the electron spins of the atoms will be reversed, which results in the creation of electron spin-up atoms in a background gas of spin-down atoms. The atoms in the upper hyperfine states, created by ESR in an inhomogeneous magnetic field, will be driven by magnetic forces to low magnetic field regions, or recombine with spin-down atoms. ESR pumping and subsequent ejection from a magnetic field has been proposed as a means of production of a doubly spin-polarized atomic hydrogen beam.[5] Conceivably, very pure doubly polarized hydrogen may be produced by removing the $|a\rangle$-state atoms with ESR.[6] To explore these potential applications of the ESR pumping technique, a study was made of the effect of microwave pumping on the decay of the lower hyperfine state densities. The pumping experiments were carried out in a ^{3}He-^{4}He lined sample chamber at a temperature of 160 mK and a magnetic field of 5.6 T. We shall present a model of ESR pumping and beam extraction, and compare this model with experimental results. Our model will include various processes, such as recombination, spin-exchange relaxation, diffusion, and effusion (escape from the source). Our results show that at moderate densities spin exchange plays a crucial role in relaxing the upper hyperfine states before they can be ejected, thus giving substantially different results than predicted from a more naive picture. Our model is used to analyze the limitations and the optimum operating conditions of an ESR pumped beam source.

II. A MODEL FOR THE DENSITY DECAY DURING MICROWAVE PUMPING

First we briefly discuss our experimental geometry, sketched in Fig. 1(a). The apparatus is the same as the one used by Van Yperen *et al.*[1] with some minor modifications. For a more detailed description of the apparatus, the reader is referred to this paper. The spectrometer is of a far-infrared (FIR) broad-band design, operating at a frequency of 157 GHz, and a central field of 5.6 T. It consists of a long cylindrical tube, filled with a localized sample. Changes in the transmission due to the presence of the sample are detected by a semiconductor bolometer, which operates at a temperature of 0.5 K. ESR transitions create a small population of electron spin-up atoms in the center of the magnetic field, in the middle of a background gas of spin-down atoms. In Fig. 1(a) we also depict a possible path of a spin-up atom. In Fig. 1(b) we show a calculated typical axial density distribution of the atoms in the lower hyperfine states together with the magnetic field profile. The density profile is approximately rectangular in shape, and has a length of 10 cm, extending from $z=-L_-$ to $z=L_+$. In our coordinate system $z=0$ corresponds to the center of the mag-

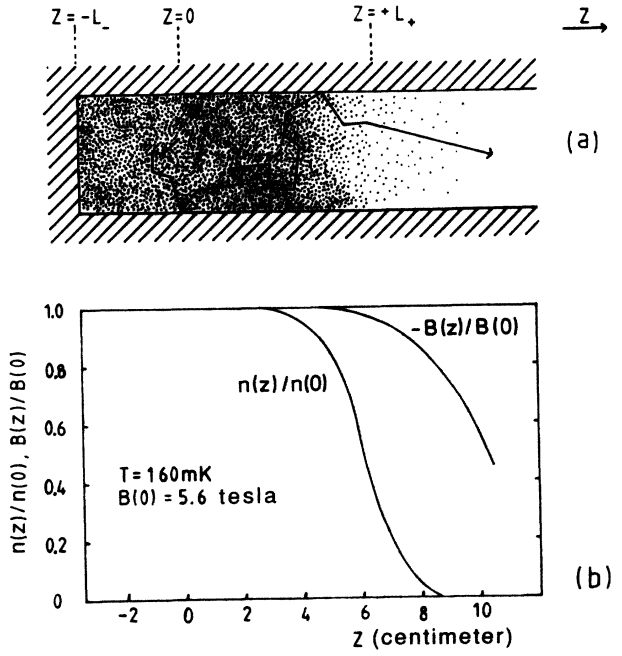

FIG. 1. (a) Experimental geometry. Electron spin-up atoms are created by ESR in a background gas of spin-down atoms. A typical path of a spin-up particle is shown. (b) Magnetic field distribution and equilibrium density distribution of the lower hyperfine states.

netic field and $z=-L_-$ corresponds to the location of a mylar window, where the density abruptly falls to zero. The width of the zone at the field center where the ESR transitions are induced is determined by the field homogeneity. At resonance, this zone has a width of about 1 cm in our system. In the following treatment we shall for simplicity assume that all transitions take place at $z=0$. To escape without recombination at the walls, the atoms with reversed spin have to traverse the zone to $z=L_+$, a distance of about 6 cm, where the field gradient is practically zero and where their motion is diffusionlike due to collisions with the background gas and the sample container walls. Collisions in the gas phase may result in spin exchange, while wall collisions may result in recombination with atoms in the lower hyperfine states. Once the spin-up atoms have left the background gas, they will be rapidly accelerated due to the field gradient.

The calculation of the temporal behavior of the densities of the four hyperfine states in the presence of a strong resonant microwave field involves the solution of four coupled partial differential equations, describing the occupation of the four hyperfine levels as a function of space and time. We use a one-dimensional treatment for simplicity. The form of these equations is governed by conservation of mass, including terms due to recombination, relaxation, ESR, and transport due to diffusion and drift in the field gradient. Using a shorthand notation a,b,c,d for $n_a(z,t)$, $n_b(z,t)$, $n_c(z,t)$, and $n_d(z,t)$, and $n=a+b+c+d$ the equations are

$$\partial a/\partial t=-2K_{aa}a^2-K_{ab}ab-K_{ac}ac-K_{ad}ad+G^{\rm imp}(b-a)+G_{\rm ex}(bd-ac)-W_{ad}^{\rm ESR}(a-d)-\partial J_a/\partial z+G_{ad}^{\downarrow}nd\ , \tag{1a}$$

$$\partial b/\partial t=-K_{ab}ab-K_{bc}bc-K_{bd}bd-G^{\rm imp}(b-a)-G_{\rm ex}(bd-ac)-W_{bc}^{\rm ESR}(b-c)-\partial J_b/\partial z+G_{bc}^{\downarrow}nc\ , \tag{1b}$$

$$\partial c/\partial t=-2K_{cc}c^2-K_{ac}ac-K_{bc}bc-K_{cd}cd+G_{\rm ex}(bd-ac)+W_{bc}^{\rm ESR}(b-c)-\partial J_c/\partial z-G_{bc}^{\downarrow}nc\ , \tag{1c}$$

$$\partial d/\partial t=-K_{ad}ad-K_{bd}bd-K_{cd}cd-G_{\rm ex}(bd-ac)+W_{ad}^{\rm ESR}(a-d)-\partial J_d/\partial z-G_{ad}^{\downarrow}nd\ . \tag{1d}$$

The K's refer to the two-body surface-recombination rate constants. As the densities in our experiments do not exceed a value of 10^{16} cm^{-3}, we neglect all three-body terms. The impurity-relaxation rate constant for the lower hyperfine states is denoted by $G^{\rm imp}$; $G_{ad}^{\downarrow}$ and $G_{bc}^{\downarrow}$ are the two-body dipolar relaxation rate constants for $d\rightarrow a$ and $c\rightarrow b$ relaxation.[7] We neglect two-body dipolar relaxation of the lower hyperfine states, as it is dominated by impurity relaxation in our experiments. The rate constant for spin-exchange relaxation is given by $G_{\rm ex}$. In a strong magnetic field, the only spin-exchange channel with a nonvanishing cross section involves collisions between *ac* or *bd* pairs.[8] This process is normally unimportant at strong fields if the occupation of the upper hyperfine states is zero. However, in the case of a small population of the upper states, in the present case created by ESR, the spin-exchange rate may be very important. The rate constants $W_{ad}^{\rm ESR}$ and $W_{bc}^{\rm ESR}$ represent the transition rates due to ESR; as outlined before, we assume that all transitions take place at $z=0$ or $W^{\rm ESR}(z)=W^{\rm ESR}\delta(z)$, with $\delta(z)$ the δ function. As spin-up atoms after generation by ESR may relax back to the lower hyperfine states, the effective generation rate is reduced. For this reason we will not treat these relaxation terms explicitly, but rather include them in the net ESR generation rates. Finally, J_a, J_b, J_c, and J_d are the current densities due to diffusion or migration; their form will be discussed in the following sections.

In the following we shall solve these equations with a simple approximate model, rather than finding a rigorous solution, for instance, by means of a Monte Carlo simulation. The analysis yields a rather simple picture in terms of a few characteristic lengths, and explains all of the salient features of the pumping experiments. We estimate the accuracy of our model to be of the level of tens of percent.

In our experiments, to be described later, with a moderately strong microwave power of about 100 nW, it takes at least 100 sec to remove the sample. With equal occupations of the four hyperfine states, the gas has a lifetime of a fraction of a second at a total density of 10^{16} cm^{-3}. This implies that the densities of the upper hyperfine states are small compared to the lower

hyperfine state densities. This considerably simplifies the analysis. The recombination terms in Eqs. (1a)–(1d) containing products of upper hyperfine state densities and the contributions of these states to the ESR transition rates may be neglected. Furthermore, we treat the density distributions as quasistationary, neglecting transient effects such as switching on the microwave field. This allows us to effectively decouple the time and the spatial dependence of the densities. To justify this step, we estimate the time required to build up a stationary density in the upper hyperfine states. After a time t, the spin-up atom has diffused over an average distance $\langle z \rangle = (2Dt)^{1/2}$, where D is the diffusion coefficient. An electron spin-up atom therefore roughly spends a time $\tau = L_+^2/2D$ in the background gas before it escapes to a low field. We find $\tau = 0.1$ sec at a total density of 10^{16} cm^{-3} (a more detailed discussion of diffusion processes will be given later). After switching on the microwave field, the density in the upper hyperfine states builds up with the same time constant τ. As the total density decays on a much slower time scale, we may regard the spatial density distributions as quasistationary. Thus we may proceed in two steps: first calculate the density distributions, neglecting the time derivatives of the densities in equations (1a)–(1d), and then solve the rate equations for the densities, averaged over the spatial distributions. Our final object will be the calculation of the recombination losses, the intensity of the emerging beam of spin-up atoms, and the nuclear polarization of the beam.

III. DENSITY DISTRIBUTIONS

Our system, sketched in Fig. 1(b), may be divided into three parts: the central part where the field gradient is vanishingly small, a zone where the field falls off approximately linearly, and a zone where the field is almost zero. Spin-up atoms, entering the zero-field region, will eventually recombine there, as they have a small probability to return to the field center. We assume that all densities are zero in the zero-field region and also neglect the tail in the density distribution of the lower hyperfine states beyond $z = L_+$. We approximate the real field distribution by a field having a trapezoidal shape,

$$B(z) = \begin{cases} B(0), & z < L_+ \quad (2a) \\ B(0)[1-(z-L_+)/\Delta z], & L_+ < z < L_+ + \Delta z \quad (2b) \\ 0, & z > L_+ + \Delta z \quad (2c) \end{cases}$$

where Δz is the distance over which the field drops from its maximum value to zero. In our geometry the field gradient has a value of approximately 1 T cm and $\Delta z = 5.6$ cm.

In the central portion of the density distribution, the atomic motion is diffusive, and the current density is of the form $J = -D\partial n/\partial z$, where D is the diffusion coefficient. The differential equations for the quasistationary density distributions of the upper hyperfine states follow from Eqs. (1c) and (1d). Retaining only the leading term, we get

$$D(d^2/dz^2)c(z) = K(a+b)c(z) + G_{ex}[ac(z) - bd(z)] , \quad (3a)$$

$$D(d^2/dz^2)d(z) = K(a+b)d(z) - G_{ex}[ac(z) - bd(z)] . \quad (3b)$$

G_{ex} is the spin-exchange rate constant and we have assumed that all recombination processes between spin-up and spin-down atoms have a common rate constant K. Using a spin-exchange cross section of 1Å^2 (Ref. 9) we find $G_{ex} = 8.2 \times 10^{-13}$ cm^3/sec. The surface recombination rate has been measured by Jochemsen *et al.*[10] for a ^{3}He surface and by Van Yperen *et al.*[11] for ^{3}He-^{4}He mixtures. Using a binding energy of 0.39 K and a two-dimensional cross length of 0.18 Å for all processes involving a spin-up and a spin-down particle we find $K = 2.3 \times 10^{-15}$ cm^3/sec at a field of 5.6 T and a temperature of 0.16 K.

Both particle-wall and particle-particle collisions contribute to the diffusion coefficient. The overall diffusion is estimated by simply adding the flow impedance due to both kinds of collisions; this gives

$$1/D = 1/D_0 + 1/D_k , \quad (4)$$

where $D_k = (\frac{2}{3})a\bar{v}$ is the Knudsen diffusion constant (a is the tube radius and $\bar{v}$ the thermal velocity). Here we neglect specularity in atom-wall collisions as observed by Berkhout *et al.*[12] This seems justified as no particular care was taken to obtain a flat substrate for the helium film. Our results are not too sensitive to the value of the diffusion coefficient. We use $D_0(a+b) = 1.8 \times 10^{18}$ cm^{-1} sec^{-1}.[13]

Another set of two equations, similar to Eqs. (3a) and (3b), holds for the lower hyperfine state distributions, with additional terms for $a-a$ and $a-b$ recombination and $b-a$ relaxation. To create spin-up atoms at $z = 0$, a supply of down-state atoms by diffusion is needed. The density gradients in the four hyperfine states are therefore of the same order of magnitude. Assuming that the densities of the upper states are small compared to the lower-state densities, one expects that the presence of the upper-state distributions will cause a relatively small density variation along the z axis in the lower states. We shall neglect this perturbation of the lower states. Then the spin-down distributions reduce to the equilibrium distributions, sketched in Fig. 1(b), which we approximate by a rectangular distribution, extending from $z = -L_-$ to $z = +L_+$.

It is instructive to introduce three characteristic length scales to express the relative importance of recombination and spin-exchange phenomena,

$$L_{rec} = [D/(K(a+b))]^{1/2} , \quad (5a)$$

$$L_{ex}^c = [D/(G_{ex}a)]^{1/2} , \quad (5b)$$

$$L_{ex}^d = [D/(G_{ex}b)]^{1/2} . \quad (5c)$$

In terms of these quantities, Eqs. (3a) and (3b) may be rewritten,

$$(d^2/dz^2)c(z) = (L_{\rm rec})^{-2}c(z) - (L_{\rm ex}^c)^{-2}c(z) + (L_{\rm ex}^d)^{-2}d(z) , \quad (6a)$$

$$(d^2/dz^2)d(z) = (L_{\rm rec})^{-2}d(z) + (L_{\rm ex}^d)^{-2}c(z) - (L_{\rm ex}^d)^{-2}d(z) . \quad (6b)$$

The physical meaning of $L_{\rm rec}$, $L_{\rm ex}^c$, and $L_{\rm ex}^b$ may be understood as follows. A lifetime $\tau=(Kn)^{-1}$ is associated with the recombination process, corresponding to an average diffusion length of $(2D\tau)^{1/2}$. The quantity $L_{\rm rec}$ may thus be regarded as the typical distance a spin-up particle drifts in the axial direction before it is lost by recombination with a down-state atom. Similar considerations apply to $L_{\rm ex}^c$ and $L_{\rm ex}^d$. From Eqs. (6a) and (6b) it is clear that these lengths determine the contours of the density distributions.

The density dependence of all relevant characteristic lengths is plotted in Fig. 2. At all densities a constant nuclear polarization $n_b/n_a=5$ has been assumed. At low densities ($<10^{14}$ cm^{-3}) the particles principally collide with the walls, and the mean-free path is of the order of the diameter of the sample chamber; in this density regime $L_{\rm rec}$, $L_{\rm ex}^c$, and $L_{\rm ex}^d$ are proportional to $n^{-1/2}$. In the high-density regime ($>3\times10^{15}$ cm^{-3}) collisions in the gas phase dominate and these lengths, together with the mean-free path λ are proportional to n^{-1}. In Fig. 2 the asymptotic behavior at low and high densities is also shown (dashed line). From the figure it is easy to observe which processes are important at a given density. If the corresponding characteristic length is longer than L_+, the width of the distribution, then the particle may escape, without getting involved in the process under consideration (recombination or spin exchange).

The experiments were carried out in the density regime of 10^{15}–10^{16} cm^{-3}, where $L_{\rm rec}\simeq L_+$; from the behavior of $L_{\rm ex}^c$ and $L_{\rm ex}^d$ it is clear that a flipped spin is involved in several spin-exchange collisions before it is ejected.

Adding Eqs. (6a) and (6b) gives a simple differential equation for the total spin-up distribution in the central field region,

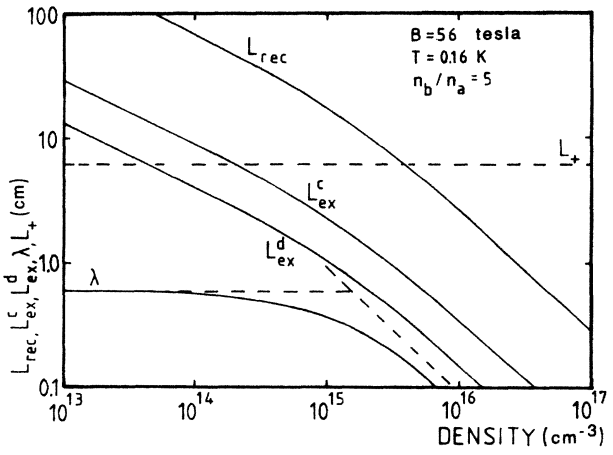

FIG. 2. Density dependence of the characteristic lengths $L_{\rm rec}$, $L_{\rm ex}^c$, $L_{\rm ex}^d$, and the mean-free path λ. Also shown is the characteristic length scale of the experimental geometry (L_+).

$$(d^2/dz^2)[c(z)+d(z)] = L_{\rm rec}^{-2}[c(z)+d(z)] . \quad (7)$$

The solution of this equation is a sum of exponentials.

In the region $z>L_+$, the spin-up particle are driven to low-field regions by the density and field gradients. The diffusional motion is slowed down by wall collisions. In a field gradient, the atoms move with a drift velocity $\mu\,|\,{\rm grad}B\,|$. Here the mobility μ is given by

$$\mu = D_k\mu_B/k_BT , \quad (8)$$

where D_k is the Knudsen diffusion constant and μ_B the Bohr magneton. Summing the contributions from the density gradient (diffusion) and the field gradient (drift) leads to the following expression for the current density:

$$J = -D_k dn^{\uparrow}(z)/dz - n^{\uparrow}D_k\mu_B/k_BTdB/dz , \quad (9)$$

where $n^{\uparrow}=n_c+n_d$. Since there is no loss of particles due to recombination, the current density should be independent of z. This leads to the following differential equation for the density distribution:

$$d^2n^{\uparrow}/dz^2 - 1/L_B dn^{\uparrow}/dz = 0 . \quad (10)$$

The spin-up density falls off exponentially in this region with characteristic length L_B, where $1/L_B = -\mu_B/k_BTdB/dz$. For our geometry L_B has a value of 0.24 cm. The solution of (10), satisfying the boundary condition $n^{\uparrow}(L_+ + \Delta z)=0$, is given by

$$n^{\uparrow}(z) = [n^{\uparrow}(L_+)/(f-1)]\{f - \exp[(z-L_+)/L_B]\} , \quad (11a)$$

$$f = \exp[\mu_B B(0)/k_BT] . \quad (11b)$$

The resulting particle flux Φ, flowing from L_+, is given by

$$\Phi = AD_k/L_B[f/(f-1)]n^{\uparrow}(L_+) \simeq AD_k n^{\uparrow}(L_+)/L_B . \quad (12)$$

Here A is the cross sectional area of the tube.

The last step in finding the spin-up density distribution is to match the solution in the gradient-free region and the density distribution in the gradient zone. The distributions must satisfy the following boundary conditions: (i) No flux at the location of the mylar window, i.e., $d(n_c+n_d)/dz=0$ for $z=-L_-$; (ii) the sum of the fluxes at $z=0$ in the positive and negative z direction equals the ESR generation rate; and (iii) the density distributions and the particle flux are continuous functions of z, except at $z=0$, where a discontinuity exists in the flux.

The spin-up density at the field center may be found by solving the coupled equations (1a)–(1d). A typical spin-up distribution is shown in Fig. 3. The estimated density of the upper hyperfine states at $z=0$ under conditions typical for our pumping experiments is of the order of 10^{12} cm^{-3}.

To calculate the individual $|c\rangle$ and $|d\rangle$ state distributions, the coupled differential equations (6a) and (6b) have to be solved. It follows from our analysis that the individual distributions differ from the sum distribution

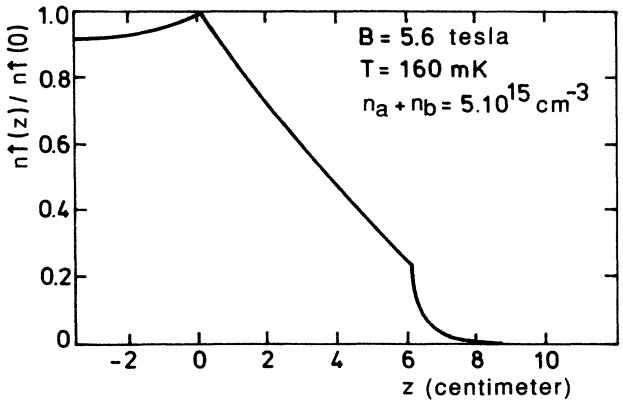

FIG. 3. Normalized spin-up density distribution.

in a region near $z=0$ of width L_{ex}^{c} or L_{ex}^{d} due to the spin-exchange terms. The distribution of the state which is created by ESR shows a peak, more pronounced than the maximum of the sum distribution, whereas the other state shows a dip at this location. Since in our experiment L_{ex}^{c} and $L_{ex}^{d} \ll L_{+}$, we may with reasonable accuracy set the individual distributions equal to the sum distribution.

Once the density distributions are known for the various hyperfine levels, the losses due to recombination and the particle flux due to ejection at $z=L_{+}$ are easily calculated as a function of the total density of the lower hyperfine states. As the density distributions of the $|c\rangle$ and $|d\rangle$ states are the same, it is convenient to express the ejection fluxes Φ_c and Φ_d in terms of the time τ_v spent by the atoms in the background gas between generation by ESR and ejection by the field, and V, the volume associated with the spin-up density distribution,

$$\Phi_c = cV/\tau_v \ , \tag{13a}$$

$$\Phi_d = dV/\tau_v \ . \tag{13b}$$

Here c and d refer to the upper hyperfine state densities at $z=0$. The expression for τ_v follows from Eq. (12),

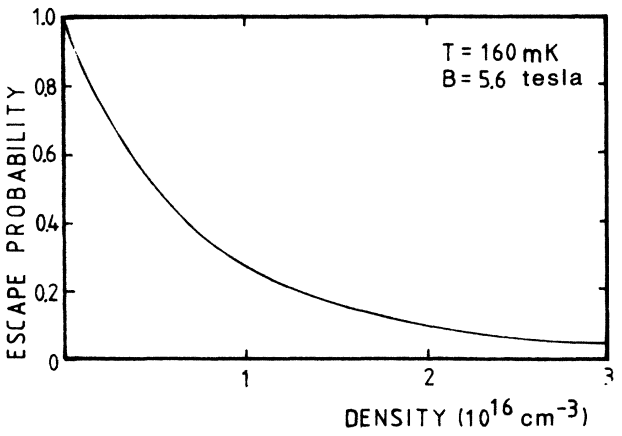

FIG. 4. Calculated escape probability for a spin-up particle vs the density of the lower hyperfine states.

$$\tau_v = (V/A)[n^{\uparrow}(0)/n^{\uparrow}(L_{+})](L_B/D_k) \ . \tag{14}$$

The time constant τ_v is a function of the total density only. In Fig. 4 we plot the probability that a spin-up particle, after generation by ESR, will be ejected (i.e., not lost by recombination with a spin-down particle). The escape probability is small if the total density exceeds a value of 10^{16} cm^{-3}. If a high flux is wanted, the total density should remain below this value.

The calculated flux of ejected particles as a function of the total density at a constant microwave power level is shown in Fig. 5. A constant density ratio $n_b/n_a = 5$ has been assumed. The effect of spin-exchange relaxation is clearly visible in the fluxes at densities of 10^{15} cm^{-3} and above, where $\varphi_c/\varphi_d = 5$, the same ratio as the density ratio of the lower hyperfine states. At densities of 3×10^{13} cm^{-3} and below, spin exchange is of less importance, but still visible. The maximum in the fluxes displayed at high densities results from recombination between spin-up and spin-down atoms. Thus at our current power level, the maximum flux is 5×10^{13} sec^{-1}.

IV. SOLUTION OF THE RATE EQUATIONS

Within the approximations discussed in the preceding sections, Eqs. (1a)–(1d) may be rewritten

$$da/dt = -2K_{aa}a^2 - K_{ab}ab - Ka(c+d) - W_{ad}^{ESR}a + G^{imp}(b-a) + G_{ex}(bd-ac) \ , \tag{15a}$$

$$db/dt = -K_{ab}ab - Kb(c+d) - W_{bc}^{ESR}b - G^{imp}(b-a) - G_{ex}(bd-ac) \ , \tag{15b}$$

$$dc/dt = -Kc(a+b) + W_{bc}^{ESR}b + G_{ex}(bd-ac) - c/\tau_v \ , \tag{15c}$$

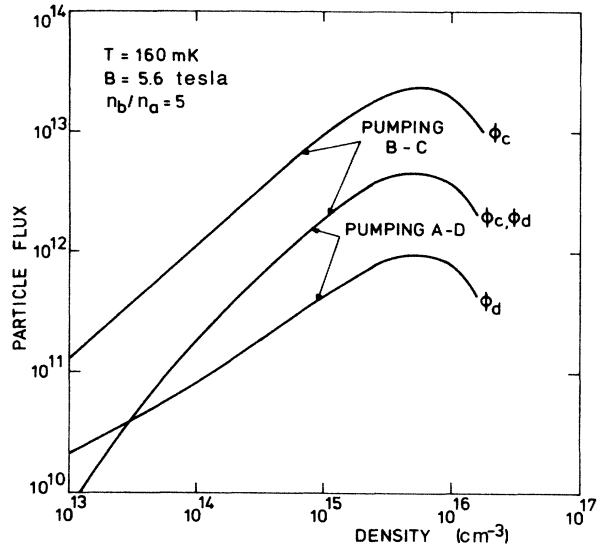

FIG. 5. Calculated flux of $|c\rangle$- and $|d\rangle$-state atoms as a function of total density and at a microwave power of 0.2 μW. A density-independent ratio $n_b/n_a = 5$ has been assumed. Note that the difference in φ_d (pumping the b-c transition) and φ_c (pumping the a-d transition) is imperceptible on this scale.

$$dd/dt = -Kd(a+b) + W_{ad}^{ESR}a - G_{ex}(bd-ac) - d/\tau_v \ . \quad (15d)$$

Here a, b, c, and d denote the densities at $z=0$. In the above equations we neglect the differences in the effective volume of the four hyperfine states. We estimate that this can introduce an error of 20%. We have ignored the diffusion terms in Eqs. 15(a) and 15(b). The values of G^{imp}, W_{ad}^{ESR}, and W_{bc}^{ESR} were obtained by fitting the calculated decay curves to the experimental data. A rather large value for G^{imp} of 3×10^{-4} sec^{-1} was necessary to obtain a good fit. For this reason, two-body dipolar $b-a$ relaxation was not included in the analysis.

The above set of equations was solved with the help of a computer. Some typical results are shown in Fig. 6 where we plot the densities of the four hyperfine states as a function of time. At the point A the microwave power, tuned to the $|b\rangle$-$|c\rangle$ transition, is switched on. At B the microwave power is switched off. Soon after pumping has started, a density of $|c\rangle$- and $|d\rangle$-state atoms is built up. Similar results are found if pumping the $|a\rangle$-$|d\rangle$ transition is simulated numerically. One finds the surprising result that ESR pumping of one of the lower hyperfine states does not change the b/a ratio, i.e., the final nuclear polarization of the lower hyperfine states turns out to be always the same, irrespective of the transition being pumped or if there is no pumping at all.

This type of behavior is a direct consequence of the spin-exchange relaxation rates, which are at least two orders of magnitude faster than all other rates. The transient behavior after switching on the microwave field may be understood as follows. Soon after one of the upper hyperfine states is created by ESR, the other is created by spin exchange; this process goes on until the net spin-exchange rate is small. The term $bd-ac$ is driven to zero by spin exchange. Only a small fraction of the atoms is in the upper hyperfine states; consequently, the populations of the lower hyperfine states do not change very much by pumping. Spin exchange thus provides a feedback mechanism, which locks the ratio c/d to the ratio b/a, unless the microwave power is so high that the density in the upper levels becomes comparable to the density in the lower hyperfine states. In our system this occurs at power levels of 1 mW and above. Then the above analysis no longer applies.

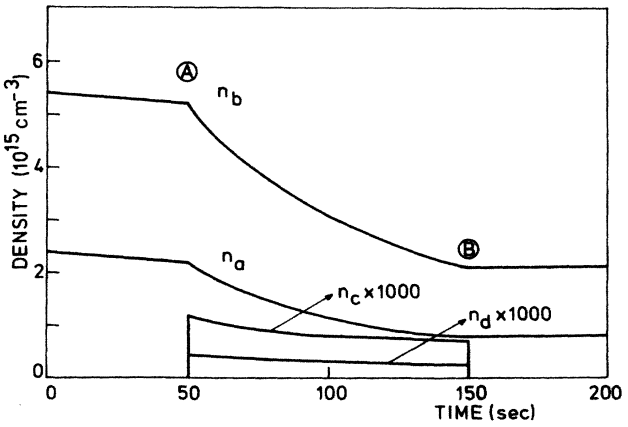

FIG. 6. Computer simulation of ESR pumping.

V. EXPERIMENTAL RESULTS

The effects of ESR pumping were studied by measuring the density decay of the lower two hyperfine states under different pumping conditions. ESR was used both to disturb the population of the four hyperfine states and to measure the density in the lower hyperfine states. To pump one of the transitions, the magnetic field was manually tuned to resonance; the densities were measured by switching the microwave frequency between the two resonance regions and sweeping the field through resonance at constant time intervals. Since it is not possible with our ESR equipment to pump one of the transitions and perform a density determination at the same time, a pressure transducer was used to monitor the total density. A constant microwave power $P_{in}\simeq0.2$ μW was used. This power level destroyed 5% of the total density every passage through resonance. No attempt was made to reduce this level since our signals were quite noisy.

The data were taken at a temperature of 160 mK, the walls of the sample container being covered by a ^{3}He-^{4}He mixture. Results are shown in Fig. 7, where we plot the measured densities n_a and n_b and the polarization $P=(n_b-n_a)/(n_b+n_a)$ as a function of time. Three situations are compared in this figure: no pumping [Fig. 7(a)], pumping the $|a\rangle$-$|d\rangle$ transition [Fig. 7(b)], and pumping the $|b\rangle$-$|c\rangle$ transition [Fig. 7(c)].

The measurement without pumping of Fig. 7(a) was taken for reference to separate the effect of pumping from the unwanted destruction by a density determination with ESR. After the cell is filled with a density of about 10^{16} cm^{-3} a moderate nuclear polarization ($n_b/n_a\simeq5$) builds up in the initial portion of the decay. Starting at a total density of 6×10^{15} cm^{-3} (point I in Fig. 7) the mi-

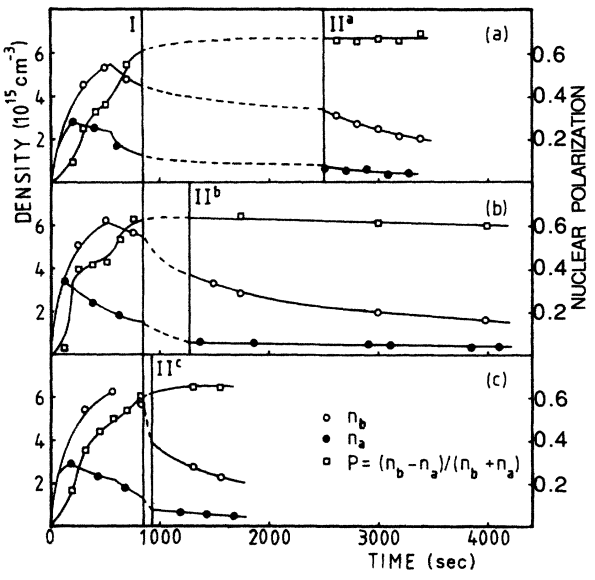

FIG. 7. Experimental results. See text for a discussion.

crowave power is switched off to allow for a free decay, undisturbed by ESR [dashed lines in Fig. 7(a)]. When the total density has fallen to a value of 3×10^{15} cm^{-3} [point II^a in Fig. 7(a)] the microwave power is switched on again to resume measuring the densities n_a and n_b.

At point I in Fig. 7(b) the power is not switched off as in Fig. 7(a), but in contrast the decay is perturbed by pumping the $|a\rangle$-$|d\rangle$ transition in the density interval 6×10^{15} cm^{-3}–3×10^{15} cm^{-3} [dashed line in Fig. 7(b)]. This increases the decay rate by a factor of 4, the final polarization turns out to be unchanged. In Fig. 7(c) the decay is perturbed by pumping the $|b\rangle$-$|c\rangle$ transition in the same density interval. This results in the most rapid decay, since the rate at which spin-up particles are created is proportional to n_b and $n_b/n_a \simeq 5$. The final polarization is about the same in Figs. 7(a)–7(c).

Our experimental results reflect the same behavior as the numerical calculations. Therefore, we attribute the observed behavior to spin-exchange relaxation. However, from our measurements no conclusion can be drawn regarding the precise value of the spin-exchange rate constant. From our numerical calculations we estimate that the maximum ejection flux was 5×10^{13} sec^{-1}, containing c- and d-state atoms in a ratio of 5:1.

VI. POSSIBLE APPLICATIONS OF THE ESR PUMPING TECHNIQUE

The model developed in this paper may be of help in evaluating the applications of ESR pumping mentioned in the introduction. Pumping the $|a\rangle$-$|d\rangle$ transition in a fairly pure $|b\rangle$-state gas is likely to be followed by spin exchange, resulting in $|a\rangle$-$|c\rangle$ pairs. This process is inhibited at sufficiently low densities (below 3×10^{13} cm^{-3} in our geometry, see Fig. 2). Purifying a gas of $|b\rangle$-state atoms with a small $|a\rangle$-state impurity by pumping the $|a\rangle$ state is therefore restricted to low densities unless the value of L_+ is small. If we take 1 cm as a practically achievable lower bound for the width of the density distribution, then this technique will be effective up to densities of the order 10^{15} cm^{-3}. This is easily seen from Fig. 2.

Generating an atomic beam by ESR pumping seems more promising. The factors affecting the particle flux and the nuclear polarization of the emerging beam are the total density, microwave power, magnetic field, and geometry (field configuration). In this section we discuss how the best choice for each of these parameters may be found to obtain the maximum particle flux.

The temperature and the field mainly affect $L_{\rm rec}$. With a ^{3}He-^{4}He-covered sample chamber the recombination rate will be minimum at a temperature of 200 mK.[8] At this temperature, the volume and the surface contributions to the recombination rate are equal. Our experiment was performed near this optimum, so $L_{\rm rec}$ cannot be made more than a factor of 2 longer by working at a different temperature or field. The role of the field configuration (homogeneity) is expressed via L_+. A smaller value of L_+, the width of the distribution, may be obtained by reducing the homogeneity of the field. This also reduces the ESR pumping rate, which is no problem if a high-power source such as a far infrared laser or a carcinotron is available. However, in practice it will not be possible to obtain a value of L_+ much below 1 cm. The most important parameter governing both recombination and spin exchange is the density of the spin-down background gas. Recombination will be unimportant at densities below 3×10^{15} cm^{-3}; spin exchange will be unimportant below 10^{13} cm^{-3}. Optimizing the system allows for working at a higher density and results in a higher flux. One order of magnitude in operating density may be gained before recombination losses become appreciable.

To illustrate the above considerations, we estimate the ejection flux from a high-power source. A moderate homogeneity magnet coil (inhomogeneity 1×10^{-3} in a 1 cc volume) yields a value for L_+ of approximately 1 cm for a central field of 5.6 T and a temperature of 200 mK. For a density of 5×10^{16} cm^{-3} and a microwave power of 200 mW the flux is 5×10^{18} sec^{-1}.

The following conclusions apply to the nuclear polarization of the emerging beam: (i) pumping an ESR transition in an unpolarized or moderately nuclear spin-polarized background gas of high density will result in a mixture of the two upper hyperfine states in the beam; (ii) $|c\rangle$-state atoms may live relatively long in an almost pure $|b\rangle$-state environment, since there are no $|a\rangle$-state partners for spin exchange available. Pumping the $|b\rangle$-$|c\rangle$ transition therefore results in a polarized beam of $|c\rangle$-state atoms if $L_{\rm ex}^c \gg L_+$; (iii) pumping the $|a\rangle$-$|d\rangle$ transition in an almost pure gas of $|b\rangle$-state atoms also results in a low-intensity polarized beam of $|c\rangle$-state atoms; the $|d\rangle$-state atoms created by ESR are quickly converted into the $|c\rangle$ state due to spin exchange but cannot relax back (they may relax to the $|b\rangle$ state by the dipolar mechanism). Thus the production of a pure $|d\rangle$-state beam is only possible at densities of 10^{14} cm^{-3} and below.

The following conclusions apply to the particle flux: (i) a high ESR pumping efficiency favors a homogeneous magnetic field, whereas a high escape probability requires a narrow density profile and thus an inhomogeneous field; (ii) if the density of the background gas exceeds a certain temperature-dependent value, pumping will be inefficient due to recombination.

VII. SUMMARY

The importance of various relaxation, recombination, and diffusion processes depends on density, temperature, magnetic field, and the width of the density distribution. It is elucidating to distinguish between the different regimes of these parameters by considering the characteristic lengths $L_{\rm rec}$, $L_{\rm ex}^c$, $L_{\rm ex}^d$, and L_+, using a plot such as Fig. 2. Recombination of spin-up and spin-down atoms is unimportant if $L_{\rm rec} \ll L_+$; similar conditions hold for spin exchange with characteristic lengths $L_{\rm ex}^c$ and $L_{\rm ex}^d$. The experiments were carried out at densities of 10^{15}–10^{16} cm^{-3}, where spin exchange is important for both upper hyperfine states and where $L_{\rm rec} \simeq L_+$. The experimental observations may be summarized as follows. Pumping one of the ESR transitions at our currently

available power levels only affects the time scale of the decay, not the nuclear polarization. We attribute this behavior to spin-exchange relaxation. This is supported by numerical estimates. From the experimental results no conclusion can be drawn regarding the precise value of the spin-exchange rate constant G_{ex}. However, the measurements clearly confirm that G_{ex} is large compared to all other terms.

ACKNOWLEDGMENTS

It is a pleasure to thank O. H. Höpfner for technical support, and R. Sprik and J. J. Berkhout for assistance with the measurements. The financial support of the Stichting voor Fundamenteel Onderzoek der Materie (FOM) and the U.S. Department of Energy Grant No. DE-FG02-85ER45190 is gratefully acknowledged.

*Present address: Hogeschool West Brabant, Postbus 90116, NL-4800 RA Breda, Noord-Brabant, The Netherlands.

†Present address: Philips Natuurkundig Laboratorium, Postbus 80000, NL-5600 JA Eindhoven, North Brabant, The Netherlands.

[1]G. H. van Yperen, J. T. M. Walraven, and I. F. Silvera, Phys. Rev. B **30**, 2386 (1984).

[2]B. W. Statt, W. N. Hardy, A. J. Berlinsky, and E. J. Klein, J. Low Temp. Phys. **61**, 471 (1985).

[3]M. W. Reynolds, I. Shinkoda, W. N. Hardy, A. J. Berlinsky, F. W. Bridges, and B. W. Statt, Phys. Rev. B **31**, 7503 (1985).

[4]M. W. Reynolds, I. Shinkoda, R. W. Cline, and W. N. Hardy, Phys. Rev. B **34**, 4912 (1986).

[5]T. O. Ninnikoski, S. Pentillä, J. M. Rieubland, and A. Rijllard, *Polarized Proton Ion Sources (Brookhaven, 1982),* Proceedings of the Conference on Polarized Proton Ion Sources, AIP Conf. Proc. No. 95, edited by G. Roy and P. Schnor (AIP, New York, 1983), p. 139; S. Pentillä, thesis, University of Turku, Finland (1985).

[6]D. Kleppner and T. J. Greytak, *High Energy Spin Physics (Brookhaven, 1982),* Proceedings of the Fifth International Conference on High Energy Spin Physics, AIP Conf. Proc. No. 95, edited by G. M. Bunce (AIP, New York, 1983), p. 546.

[7]R. Sprik, J. T. M. Walraven, and I. F. Silvera, Phys. Rev. B **32**, 5668 (1985).

[8]I. F. Silvera and J. T. M. Walraven, in *Progress in Low Temperature Physics,* edited by D. Brewer (North-Holland, Amsterdam, 1986), Vol. X, Chap. D.

[9]A. J. Berlinsky and B. Shizgal, Can. J. Phys. **58**, 881 (1980); M. Morrow and A. J. Berlinsky, *ibid.* **61**, 1042 (1983).

[10]R. Jochemsen, M. Morrow, A. J. Berlinsky, and W. N. Hardy, Phys. Rev. Lett. **47**, 852 (1981).

[11]G. H. van Yperen, A. P. M. Matthey, J. T. M. Walraven, and I. F. Silvera, Phys. Rev. Lett. **47**, 800 (1981).

[12]J. J. Berkhout, E. J. Wolters, R. van Roijen, and J. T. M. Walraven, Phys. Rev. Lett. **57**, 2387 (1986).

[13]J. P. Bouchaud and C. Lhuillier, J. Phys. **46**, 1781 (1985).